IEEE Access
Multidisciplinary | Rapid Review | Open Access Journal

Received January 25, 2021, accepted May 27, 2021, date of publication June 2, 2021, date of current version June 14, 2021.

Digital Object Identifier 10.1109/ACCESS.2021.3085236

Improving Harmonic Rejection Capability of OSG Based on n-th Order Bandpass Filter for Single-Phase System

YE GU KANG, (Member, IEEE), AND DAVID DIAZ REIGOSA, (Member, IEEE)
Department of Electrical Engineering, University of Oviedo, 33204 Gijon, Spain

Corresponding author: Ye Gu Kang (kangyegoo@gmail.com)

This work was supported in part by the Research, Technological Development and Innovation Programs of the Spanish Ministry Economy and Competitiveness, under Grant MCI-20PID2019-106057RB-I00.

ABSTRACT The second-order generalized integrator based orthogonal signal generator (SOGI-OSG) is commonly used to produce direct and quadrature axis (dq-axes) signals in stationary reference frame for single-phase systems. Fast and robust OSG with harmonic rejection capability is required for parallel operation of power generation systems. The frequency response function (FRF) of classical OSG does not show robustness towards DC offset and grid harmonic disturbances compared to the direct signal of SOGI. This paper presents OSGs based on n^{th} order bandpass filter with a phase shifter using a scaled Q factor as a design variable. The frequency and time-domain performance analysis will be performed based on the scaled Q factor to simplify the design process of the proposed OSGs. The -3dB frequency and settling step time will be matched in higher order OSGs selecting a scaled Q factor. The proposed method will show enhanced harmonic rejection ratio of an additional -20dB with increasing OSG order with tradeoff in computational burden.

INDEX TERMS SOGI, DC offset, harmonic distortion, quadrature signal generator.

I. INTRODUCTION

Phase-locked loop (PLL) is required in a wide variety of AC applications including single-phase system control. This includes grid-tied photovoltaic systems, rectifier loads, battery chargers, and motor drives [1]–[4]. For power quality of grid system in parallel operation, fast and robust PLL with Orthogonal Signal Generator (OSG) is required to control phase, frequency [5], magnitude [6], while it rejects harmonics including interharmonics [7], [8] and DC offset [9]. Figure 1 (a) shows the three main parts of a PLL: a phase detector (PD) with OSG and reference transformation block, a loop filter (LF) with proportional-integral (PI) controller, and a voltage-controlled oscillator (VCO) where v_{in} is the single-phase input, ω_{ff} is the feedforward frequency of the nominal grid frequency, $\hat{\omega}_s$ is the estimated input signal frequency and $\hat{\theta}$ is the estimated phase [10]. The LF estimates the input frequency which is the input of the VCO which estimates the phase angle with the initial frequency feedforward, ω_{ff}. $\hat{\omega}_s$ is feedback to the OSG for grid frequency drift adaptation, which increases the implementation complexity and also affects the stability. To overcome aforementioned issue, fixed-frequency OSG PLL are proposed ensuring stability and simple implementation [11], [12]; Figure 1 (b) shows fixed-frequency OSG with phase compensator (PC).

Second-order generalized integrator (SOGI) based OSG provide a satisfying performance compromise between the dynamic response and computational complexity [13]–[15]. The SOGI based OSG is shown in Fig. 2 (a). The SOGI-OSG generates the direct signal, v_α, and the orthogonal signal, v_β, in the stationary reference frame, which later are used as inputs to the rotating transform block, i.e., $\alpha\beta$ to dq.

However, the orthogonal output of the SOGI based OSG results in errors when the signal contains low-frequency harmonics, i.e., DC offset and interharmonics. The phase angle estimation performance degrades, which results in frequency oscillations.

To solve the SOGI-OSG problem, several methods have been proposed in the literature [9], [16]–[19]. To attenuate the interharmonics, differentiators are included in transfer function near zero frequency. The DC offset and the interharmonics are attenuated by 20 decibels every differentiator. A cascaded SOGI (SO-SOGI) PLL with a fourth-order transfer function is proposed with a differentiator in the OSG

The associate editor coordinating the review of this manuscript and approving it for publication was Xiaoli Luan.

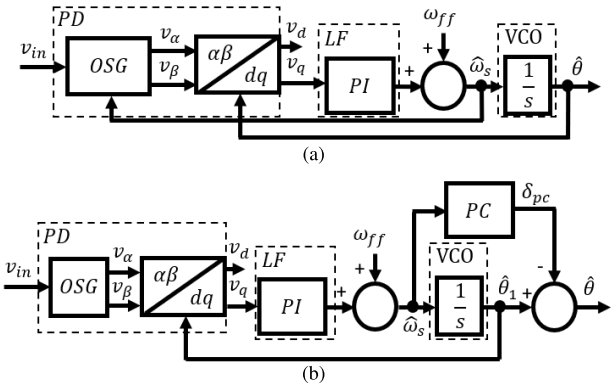

FIGURE 1. Single phase OSG-PLL. (a) SOGI-OSG PLL. (b) Fixed-frequency OSG PLL with phase error compensation feedforward.

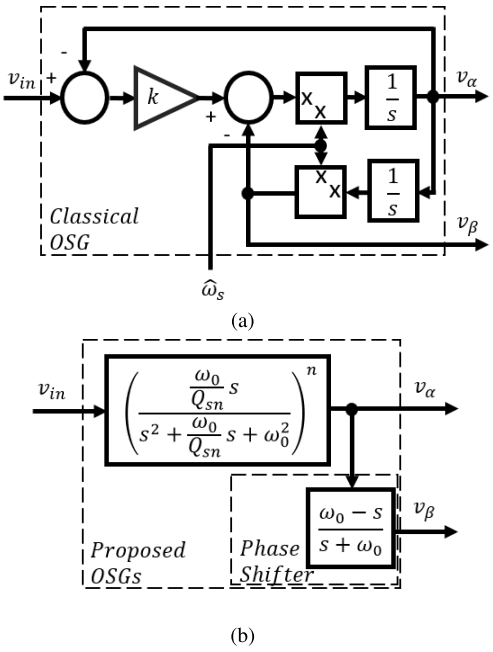

FIGURE 2. OSGs. (a) SOGI-OSG. (b) Proposed OSG with n^{th}-order BPF.

in [16]. The modified SOGI (MSOGI-PLL) with an additional filter block is proposed to remove the DC offset component causing constant error [17]. These techniques, however, showed asymmetric harmonic rejection capability on the low and high-frequency range. For this reason, the direct and the orthogonal component has different harmonic rejection capability. In [9], a mixed second and third-order SOGI (MSTOGI-PLL) is proposed with symmetric harmonic rejection property on both direct and orthogonal axes components. A comparative survey on the OSG based PLL is presented in [10], [20], [21] with voltage sag, frequency step, phase jump, and DC offset rejection capability.

In this paper, OSGs with n^{th}-order bandpass filter (BPF) with scaled Q (Quality) factor, Q_{sn}, are proposed with a phase shifter, see Fig. 2 (b). The conclusions on Q factor

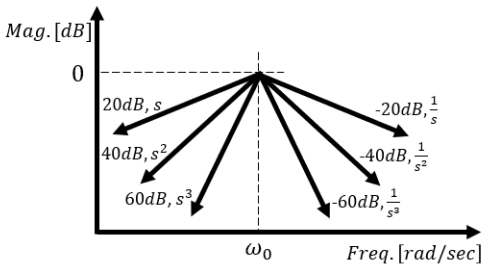

FIGURE 3. Integrators and differentiators and FRF slope in dB.

in general filter theory is reused [22], [23]. Scaled Q factors for higher order OSGs are proposed to simplify the design process of the higher order OSGs, i.e., second and third order. It will be shown that the proposed OSGs enhance harmonic rejection property while ensuring fast dynamics. An additional −20dB of the harmonic rejection will be achieved with every increasing filter order, as shown in Fig. 3. Both time-domain and frequency-domain analysis are performed for the second- and the third-order OSGs. The proposed OSGs are adopted to fixed-frequency OSG-PLL in Fig. 1 (b) introducing lookup table (LUT) based phase compensator to adapt input frequency drift. Stability analysis is included for the fixed-frequency PLL based on the proposed OSGs.

The paper is organized as follows: Section II compares harmonic rejection ability of SOGI-based OSGs and the proposed OSGs, summarizing the tradeoff between filtering ability and computational burden; in section III, the proposed OSGs based on n_{th}-order BPF with scaled Q factor is introduced with time- and frequency-domain analysis; section IV shows the implementation of the PLL using the proposed OSGs; section V, shows the simulation and experimental results to demonstrate the advantages of the proposed OSG; finally section VI presents the conclusions of the paper.

II. SOGI BASED OSGs AND BPF OSGs COMPARISON

In this section, the harmonic rejection capability of existing SOGI-OSG and the proposed OSGs based on n^{th}-order BPF is compared considering computational burden. SOGI-OSG [13], [14], CSOGI-OSG [16], MSOGI-OSG [17], Differential SOGI-OSG [24], and MSTOGI-OSG [9] are compared with the proposed OSGs. Summary of harmonic filtering ability and computational burden are shown in Table 1.

Figure 3 presents the slope of the Frequency Response Function (FRF) of OSGs in decibel (dB) with target frequency, ω_0. Comparing the highest and lowest order complex variable, s^n, in numerator and denominator of FRF, the harmonic rejection capability can be presumed. Additional s^n in the numerator results in additional 20dB of harmonic rejection capability in low frequency range where additional $1/s^n$ in denominator results in additional −20dB in high frequency range as shown in Fig. 3.

TABLE 1. OSGs harmonic rejection ability and computational burden comparison.

Technique	DC		Low frequency		Target frequency		High frequency		Computational burden	
	α	β	α	β	α	β	α	β	X [a]	+ [b]
SOGI-OSG [13], [14]	0	k	20dB	0dB	1	1	-20dB	-40dB	9	7
CSOGI-OSG [16]	0	0	40dB	20dB	1	1	-40dB	-60dB	15	13
MSOGI-OSG [17]	0	0	40dB	20dB	1	1	-20dB	-20dB	14	12
Differential-OSG [24]	0	0	20dB	40dB	1	1	-20dB	0dB	9	7
MSTOGI-OSG [9]	0	0	20dB	20dB	1	1	-20dB	-20dB	11	9
1^{st} bandpass OSG	0	0	20dB	20dB	1	1	-20dB	-20dB	11	9
2^{nd} bandpass OSG	0	0	40dB	40dB	1	1	-40dB	-40dB	18	16
3^{rd} bandpass OSG	0	0	60dB	60dB	1	1	-60dB	-60dB	25	24

[a]"X" represents number of multiplications required per sampling period.
[b]"+" represents number of additions required per sampling period.

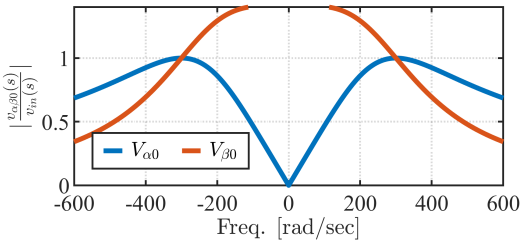

FIGURE 4. SOGI and OSG, k = 1.41, ω_0 = 300rad/sec.

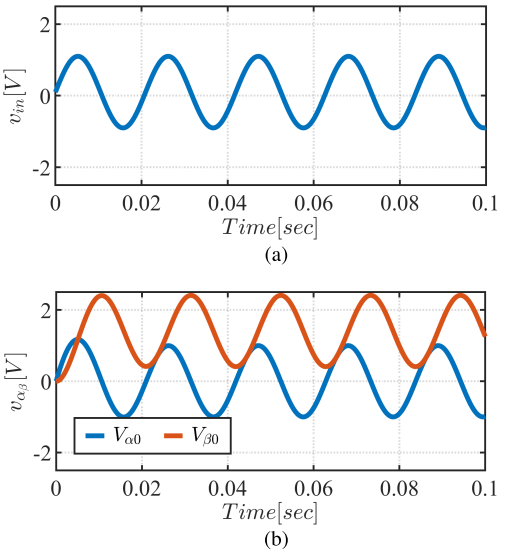

FIGURE 5. SOGI based OSG time-domain response with DC offset input, k = 1.41. (a) Sinusoidal input with DC offset, v_{DC} = 0.1V, ω = 300 rad/sec. (b) $v_{\alpha 0}$ and $v_{\beta 0}$.

A. SOGI-OSG [13], [14]

SOGI based OSG transfer functions are shown in (1), (2) where k is the half of damping factor, and $v_{\alpha 0}$ and $v_{\beta 0}$ are the filtered direct and orthogonal signals [13], [14]. The smaller the value of the gain k, the more selective response of the system; however, the filter will require a longer stabilization time [5], [25]. In further analysis of OSGs, k, is set to 1.41. Figure 4 shows the FRF plot of (1), (2) where ω_0 is set to 300rad/sec. As can be observed in the FRF plot, the DC offset or interhamonics will not be filtered in the orthogonal signal, β_0. DC offset or interhamonics will appear on the orthogonal signal as in Fig. 5 to result in performance degradation of PD.

$$\frac{v_{\alpha 0}(s)}{v_{in}(s)} = \frac{k\omega_0 s}{s^2 + k\omega_0 s + \omega_0^2} \tag{1}$$

$$\frac{v_{\beta 0}(s)}{v_{in}(s)} = \frac{k\omega_0^2}{s^2 + k\omega_0 s + \omega_0^2} \tag{2}$$

B. MODIFIED SOGI-OSG

1) CSOGI-PLL [16]

In CSOGI-OSG, two SOGIs are put in series to improve the harmonic rejection capability in Fig. 6 (a). The direct and the orthogonal signal filter transfer function are shown in (3) and (4). The modified OSG includes a differentiator to reject interharmonics. However, the low- and the high-frequency harmonic rejection ratio is asymmetric with 20dB at low-frequency and −60dB at high-frequency, respectively. The direct signal has a symmetric harmonic rejection capability with 40dB at low frequency and −40dB at high frequency.

$$\frac{v_{d1}(s)}{v_{in}(s)} = \frac{(k\omega_0 s)^2}{(s^2 + k\omega_0 s + \omega_0^2)^2} \tag{3}$$

$$\frac{v_{q1}(s)}{v_{in}(s)} = \frac{k^2\omega_0^3 s}{(s^2 + k\omega_0 s + \omega_0^2)^2} \tag{4}$$

2) MSOGI-OSG [17]

The MSOGI-OSG uses additional first-order filter function block to include a differentiator as in (5) and (6). The FRF of MSOGI is shown in Fig. 6 (b). The DC offset effect on OSG is removed. However, interharmonic rejection capability is not improved. Also, the performance of the OSG with k parameter related to the damping ratio is difficult to be predicted.

$$\frac{v_{\alpha 2}(s)}{v_{in}(s)} = \frac{\omega_0 s^2}{s^3 + (k + \omega_0)s^2 + \omega_0^2 s + k\omega_0^2} \tag{5}$$

$$\frac{v_{\beta 2}(s)}{v_{in}(s)} = \frac{\omega_0^2 s}{s^3 + (k + \omega_0)s^2 + \omega_0^2 s + k\omega_0^2} \tag{6}$$

3) DIFFERENTIAL SOGI-OSG [24]

Following the strategy of putting additional differentiator, a differential SOGI based OSG could be potentially used in (7) and (8) [24]. The FRF of this technique is shown

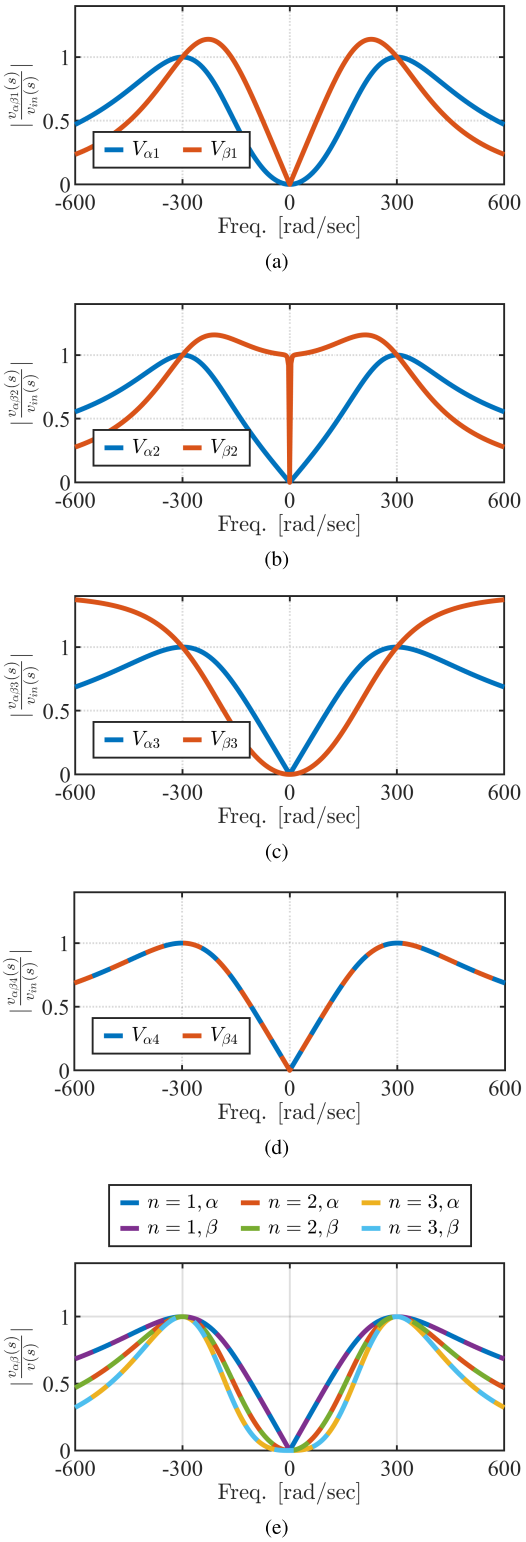

FIGURE 6. Modified OSG FRF plots $k = 1.41$, $\omega_0 = 300$rad/sec. (a) CSOGI-OSG. (b) MSOGI-OSG. (c) Differential SOGI-OSG. (d) MSTOGI-OSG. (e) Proposed OSGs.

in Fig. 6 (c). Using the proposed technique, the DC offset and the interhamonics can be filtered with 40dB, but the high harmonic component won't be rejected with 0dB. This method has the opposite characteristic compared to the SOGI based OSG.

$$\frac{v_{\alpha3}(s)}{v_{in}(s)} = \frac{k\omega_0 s}{s^2 + k\omega_0 s + \omega_0^2} \tag{7}$$

$$\frac{v_{\beta3}(s)}{v_{in}(s)} = \frac{-ks^2}{s^2 + k\omega_0 s + \omega_0^2} \tag{8}$$

4) MSTOGI-OSG [9]

Mixed second and third-order generalized integrator PLL (MSTOGI-OSG) eliminates harmonics and DC offset in the signal in (9) and (10). The FRF in Fig. 6 (d) shows symmetric harmonic attenuation capability for both low and high-frequency. The OSG is a BPF with a unity gain and 90° phase shift at the resonant frequency ω_0.

$$\frac{v_{\alpha3}(s)}{v_{in}(s)} = \frac{k\omega_0 s}{s^2 + k\omega_0 s + \omega_0^2} \tag{9}$$

$$\frac{v_{\beta3}(s)}{v_{in}(s)} = \frac{k\omega_0 s(\omega_0 - s)}{(s + \omega_0)(s^2 + k\omega_0 s + \omega_0^2)} \tag{10}$$

C. PROPOSED OSGs BASED ON n^{th}-ORDER BPF

Equation (11) and (12) show the direct and orthogonal signal transfer function of the proposed OSGs based on n^{th}-order BPF; n in (11) and (12) decides the order of OSG. Note that the orthogonal signal in (12) is composed by (11) and phase shifter (20). Phase lag or lead error of (12) and (11) are compensated by frequency drift compensator. The harmonic rejection capability of the BPF can be improved by an additional 20dB, every time that the filter order increases. Scaled Q factor, Q_{sn}, is proposed to ensure comparable time-domain response with enhanced harmonic rejection capability for higher-order OSG. Both the orthogonal and the direct signals have symmetric harmonic rejection capability and overlapped onto each other, as shown in Fig. 6 (e).

$$\frac{v_{\alpha}(s)}{v_{in}(s)} = \left(\frac{\frac{\omega_0}{Q_{sn}} s}{s^2 + \frac{\omega_0}{Q_{sn}} s + \omega_0^2}\right)^n \tag{11}$$

$$\frac{v_{\beta}(s)}{v_{in}(s)} = \left(\frac{\frac{\omega_0}{Q_{sn}} s}{s^2 + \frac{\omega_0}{Q_{sn}} s + \omega_0^2}\right)^n \left(\frac{\omega_0 - s}{s + \omega_0}\right) \tag{12}$$

D. IMPLEMENTATION OF OSGs IN DISCRETE TIME-DOMAIN

The continuous time-domain transfer function is transformed to discrete time-domain using the Tustin method with frequency pre-warping. To design discrete-time infinite-impulse-response (IIR) filters from continuous-time transfer function, Laplace variable, s, is substituted with (13) with K_w in (14) where ω_0 is the target frequency and f_{sw} is the sampling frequency of the digital-signal processor (DSP). The discrete transfer function designed using causal and stable continuous domain transfer function will preserve the stability. The number of mathematical operations required for each OSGs introduced in this section is counted and

summarized in Table 1.

$$s = K_w \frac{1 - z^{-1}}{1 + z^{-1}} \tag{13}$$

$$K_w = \frac{\omega_0}{tan(\frac{\omega_0}{2f_{sw}})} \tag{14}$$

E. SUMMARY OF OSGs ANALYSIS

A synchronous reference frame PLL (SRF-PLL) can accurately estimate the phase and frequency when the output of OSG does not present imbalance or harmonics. When grid voltage input includes imbalances or harmonics, the output of SRF-PLL will result in errors and, therefore, cannot accurately track the gird voltage phase and frequency.

Enhanced OSGs with improved harmonic rejection ability have been compared in Fig. 6 with respect to classical SOGI-PLL in Fig. 4. CSOGI-, MSOGI-, Differential SOGI-OSGs showed unbalanced frequency response between α and β components. Differential SOGI-OSG shows enhanced interharmonic rejection capability, but its performance degrades for higher order harmonics. MSTOGI and the proposed OSGs showed balanced harmonic rejection ability, yet, the proposed OSGs showed better harmonic rejection capability than MSTOGI.

It has been shown that increasing the filter order of the proposed OSG can improve the harmonic rejection capability. However, increasing the filter order results in slow dynamics response. In addition, the proposed OSG based PLL algorithm implementation becomes more complex as the filter order increases. To overcome this issue, the scaled Q factor is introduced to simplify OSG design process and guarantee a comparable dynamic performance regardless of the filter order of the OSGs. Both time- and frequency-domain analysis of the proposed OSGs will be presented in the next section (section III).

III. OSGs BASED ON n^{th}-ORDER BPF WITH SCALED Q FACTOR

In this section, n^{th}-order BPF based OSGs shown in Fig. 2 (b) is analyzed in both time- and frequency-domain. The design of the proposed OSGs starts from the notch filter and uses a scaled Q factor to help higher order OSG design. The proposed OSGs with scaled Q factor, Q_{sn}, have higher harmonic rejection capability and easy to be designed.

A. PROPOSED OSG DESIGN IN FREQUENCY-DOMAIN

Notch filter in (15) is a bandstop filter with a narrow stopband with a high Q factor [26]. The bandpass filter can be represented as a 1-notch form (see Fig. 7). Every analysis that is previously concluded on the notch filter applies to the OSG design [22], [23].

$$\frac{n(s)}{v_{in}(s)} = \frac{s^2 + \omega_0^2}{s^2 + \frac{\omega_0}{Q}s + \omega_0^2} \tag{15}$$

$$\frac{v_{\alpha(bandpass)}(s)}{v_{in}(s)} = 1 - \frac{n(s)}{v_{in}(s)} = \frac{\frac{\omega_0}{Q}s}{s^2 + \frac{\omega_0}{Q}s + \omega_0^2} \tag{16}$$

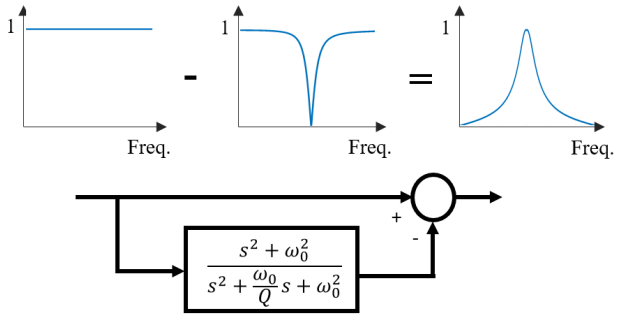

FIGURE 7. 1-Notch (bandpass) filter.

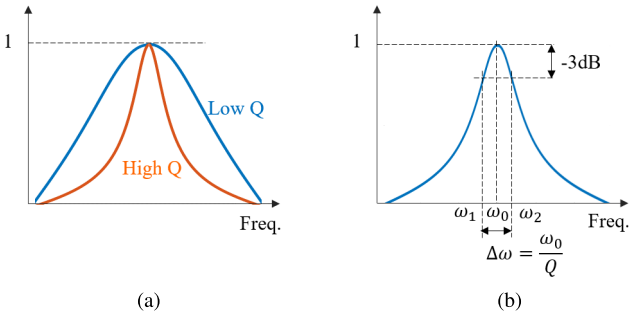

FIGURE 8. Q factor effect on FRF. (a) High and low Q factor BPF FRF. (b) Q factor and bandwidth, $\Delta\omega$.

The Q factor is a parameter that describes the resonance behavior in frequency-domain. The higher Q, the narrower the bandwidth and the higher the harmonic rejection capability (see Fig. 8 (a)). The -3dB frequency and bandwidth of the BPF can be estimated by matching (16) at -3dB frequency. By solving (17), the lower end of -3dB frequency, ω_1 and the upper end of the -3dB frequency, ω_2 shown in Fig. 8 (b) are calculated. The bandwidth of the, $\Delta\omega$, is then estimated by (21) in terms of Q factor. At the second-order filter, the -3dB frequency will be -6dB and -9dB for the third-order.

$$\left.\frac{v_{\alpha(bandpass)}}{v_{in}(s)}\right|_{-3dB} = \frac{1}{\sqrt{2}} = \frac{\frac{\omega\omega_0}{Q}}{\sqrt{(\omega_0^2 - \omega^2)^2 + (\omega_0\omega/Q)^2}} \tag{17}$$

$$\omega_1 = \omega_0 \frac{(2 \times \sqrt{Q^2 + 1/4} - 1)}{2Q} \tag{18}$$

$$\omega_2 = \omega_0 \frac{(2 \times \sqrt{Q^2 + 1/4} + 1)}{2Q} \tag{19}$$

1) PHASE SHIFTER

To achieve an orthogonal signal from a single signal, a phase shifter is used. In (20), 90° phase shifter transfer function is shown. As can be observed from Fig. 9, the shifter has unity gain in all frequency with 90° phase delay at the target frequency. The phase shifter is added to the direct signal to

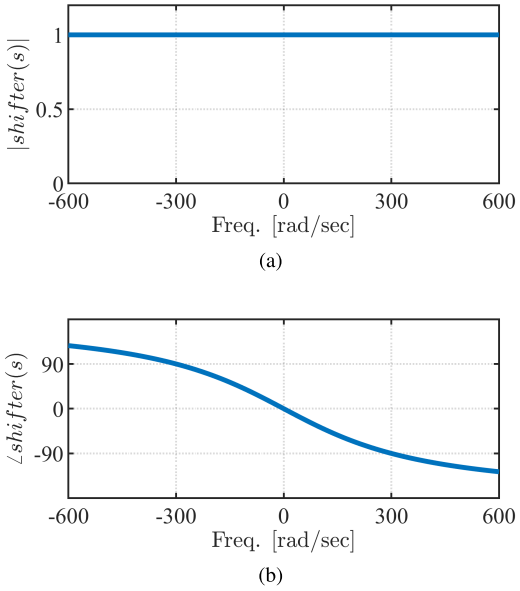

FIGURE 9. Phase shifter FRF, $\omega_0 = 300$rad/sec. (a) Magnitude. (b) Phase.

synthesize the orthogonal signal as shown in Fig. 2 (b).

$$shifter(s) = \left(\frac{\omega_0 - s}{s + \omega_0}\right) \tag{20}$$

2) SCALED Q FACTOR

Figures 10 show the first-, second-, and third-order BPF OSG FRF without scaled Q factor. Higher order OSGs show enhanced harmonic rejection ability. However, the -3dB (0.707) points of the FRF plot for higher order OSGs, which will decide setting time step response, does not match; see dashed black-line referring -3dB frequency. To match the -3dB frequency of the higher order BPF, a scaling factor is multiplied as in (21). Based on (21), scaled Q-factor, Q_{sn}, in (22) is proposed. The design of the n^{th}-order BPF can refer to Q_{sn} which will match -3dB frequency for the higher order OSGs referring to the first order OSG. Figure 11 shows the first-, second-, and third-order BPF OSG FRF designed based on the scaled Q factor. The -3dB (0.707) frequency points of the FRF plot for higher order OSGs are matching using scaled Q factor; see dashed black-line referring -3dB frequency. As can be observed, higher order OSGs based on scaled Q factor still show higher harmonic component attenuation beyond the target frequency, ω_0.

$$\Delta\omega_{\text{-3 dB}} = (\omega_2 - \omega_1) = \begin{cases} \dfrac{\omega_0}{Q}, & \text{if n=1} \\ \dfrac{\omega_0}{Q}\sqrt{2^{\frac{1}{n}} - 1}, & \text{if n>1} \end{cases} \tag{21}$$

$$Q_{sn} = \begin{cases} \dfrac{\omega_0}{(\omega_2 - \omega_1)}, & \text{if n=1} \\ Q_{s1}\sqrt{2^{\frac{1}{n}} - 1}, & \text{if n>1} \end{cases} \tag{22}$$

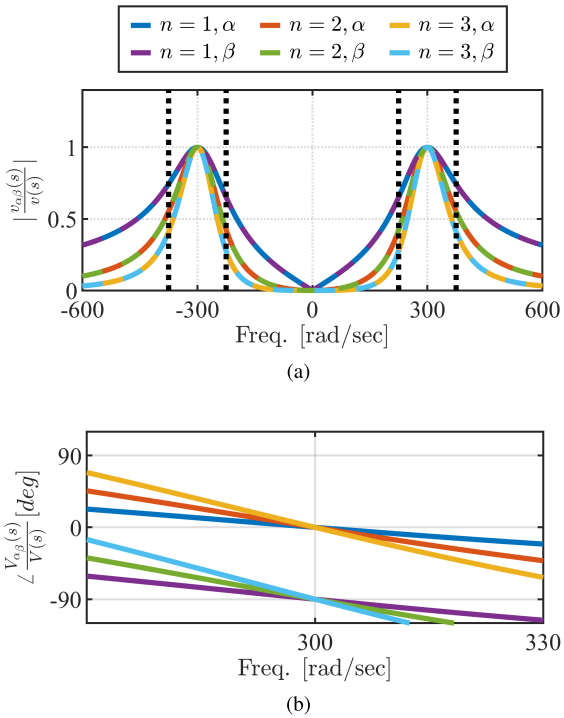

FIGURE 10. n^{th}-order BPF OSGs FRF, $Q = 2$, $\omega_0 = 300$rad/sec, dashed black-line indicate -3dB frequency. (a) Magnitude. (b) Phase.

When high Q factor is selected, harmonic rejection capability increases, see Fig. 8 (a). However, the higher the Q factor, the lower the bandwidth as shown in Fig. 8 (b). Selection of Q_{s1} factor can refer to time-domain analysis. When $n = 1$, the number of oscillation to reach 95% of the steady state value is approximately equal to Q (25). The time require to reach 95% of the steady state value can be obtained as (24). The time required for stabilizing the output of the OSGs, when a variation in its input occurs, e.g., DC offset, voltage sag, phase jump, frequency variation, etc., will be proportional to Q_{s1} (see (24)). When Q_{s1} is selected, Q_{s2} and Q_{s3} can be calculated based on (22). For example, the time to stabilizing output when Q_{s1} is equal to 2 at ω_0 of $2\pi 50$ [rad/sec], is 0.039sec. Selecting Q_{s2} and Q_{s3} equal to 1.29 and 1.01 using (22), for higher order OSGs, will also converge near 0.039sec.

$$E(t) = \begin{cases} 1 - exp\left(-\dfrac{\omega_0}{2Q}t\right), & \text{if n=1} \\ \left(1 - exp\left(-\dfrac{\omega_0}{2^{(1+n/4)}Q}t\right)\right)^n, & \text{if n>1} \end{cases} \tag{23}$$

$$t_{5p} = \begin{cases} -\dfrac{ln(0.05)2Q}{\omega_0}, & \text{if n=1} \\ -\dfrac{(ln(-0.95)^{1/n} - 1)2^{(1+n/4)}Q}{\omega_0}, & \text{if n>1} \end{cases} \tag{24}$$

$$N = \begin{cases} -\dfrac{ln(0.05)Q}{\pi} \approx Q, & \text{if n=1} \\ -\dfrac{(ln(-0.95)^{1/n} - 1)2^{(n/4)}Q}{\pi}, & \text{if n>1} \end{cases} \tag{25}$$

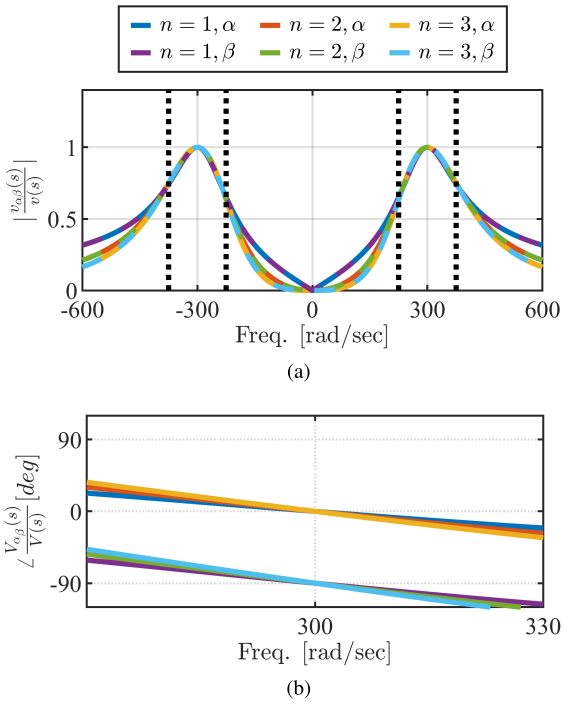

FIGURE 11. n^{th}-order BPF OSGs FRF with scaled Q factor, $Q_{s1} = 2$, $Q_{s2} = 1.29$, $Q_{s3} = 1.01$, $\omega_0 = 300$rad/sec, dashed black-line indicate −3dB frequency. (a) Magnitude. (b) Phase.

B. PROPOSED OSGs TIME-DOMAIN ANALYSIS

Q factor decides the time-domain response. The time-domain response envelops of the n^{th}-order filter is shown in (23). Using (23), the time-domain response to 5 percent settling time can be estimated as in (24). From (24), the number of oscillations required to reach the 5 percent can be obtained by (25).

Figure 12 shows the time response of (16) where Q is set to 2, 4, and 9 for the first-order BPF with the envelop in (23). The number of oscillations required for the filter output is approximately equal to the Q factor when $n = 1$; see (25). The filter order effect in time-domain response is shown in Fig. 13. Figure 13 (a) shows higher order response with constant Q factor, where (b) shows the time-domain response with scaled Q-factor. Figure 13 (a) shows slow time-domain response with increasing filter order. Using scaled Q factor in (22), higher order OSGs results in comparable dynamic response compared to first-order OSG with enhanced harmonic rejection ability as shown in Fig. 13 (b) and Fig. 11.

IV. IMPLEMENTATION OF PLLs USING THE PROPOSED OSGs

In this section, implementation and stability of the proposed OSGs based fixed-frequency PLL shown in Fig. 14 with frequency drift compensator (FDC) is introduced. LF tuning of k_i and k_p in [27] is used. ω_{ff} is set to base frequency of input, e.g., 300 rad/sec. Given input voltage, v_{in}, PD with enhanced OSG output v_q to estimate phase, $\hat{\theta}_0$. The FDC

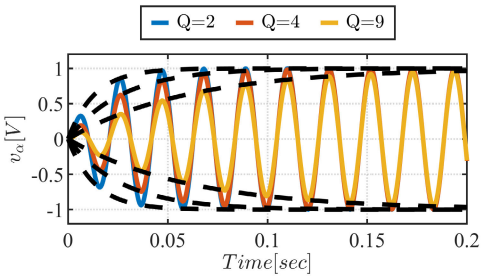

FIGURE 12. Q factor effect on time-domain response, $\omega_0 = 300$rad/sec., n = 1, Q = [2 4 9].

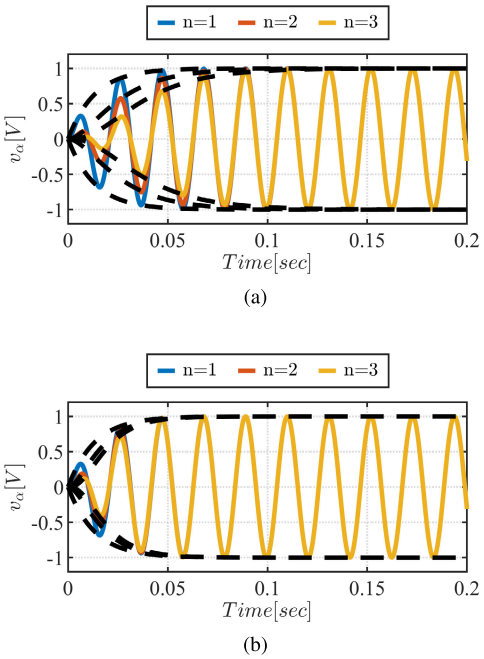

FIGURE 13. (a) n^{th}-order filter time-domain response, $\omega_0 = 300$rad/sec., n = [1 2 3], $Q = 2$. (b) n^{th} order filter time-domain response, $\omega_0 = 300$rad/sec., n = [1 2 3], $Q_{s1} = 2$, $Q_{s2} = 1.29$, $Q_{s3} = 1.01$.

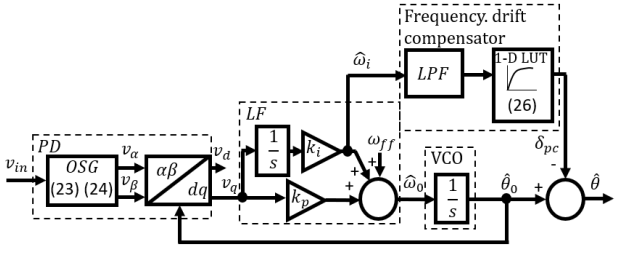

FIGURE 14. Proposed PLL based on n^{th}-order BPF OSGs with frequency drift compensator.

phase, δ_{pc}, is feedforward to compensate the frequency drift effect to finally output phase, $\hat{\theta}$.

A. FREQUENCY DRIFT ADAPTATION WITH PHASE ERROR COMPENSATOR

Figure 14 shows the implementation of FDC based on low pass filter (LPF) and 1-dimensional lookup table (1-D LUT).

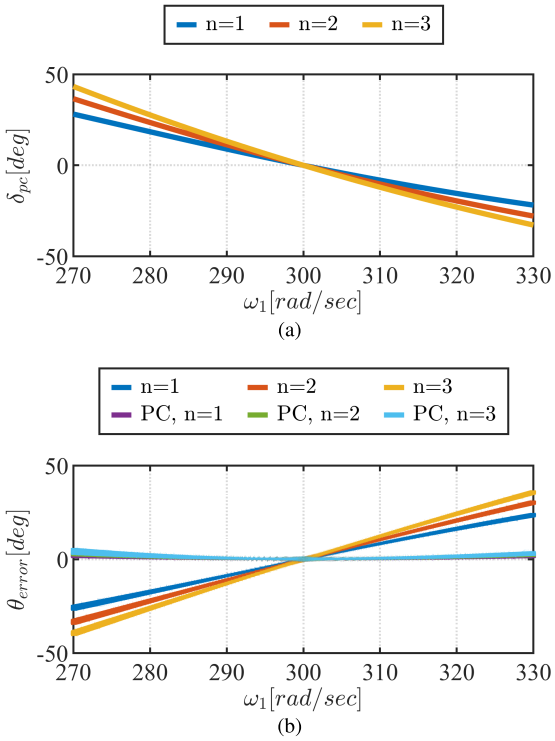

FIGURE 15. Frequency drift phase error and error compensation. (a) Phase compensation angle, δ_{pc}, with frequency drift from 270 to 330rad/sec, $\omega_0 = 300$rad/sec, $Q_{s1} = 2$, $Q_{s2} = 1.29$, $Q_{s3} = 1.01$. (b) Estimated phase error with and without frequency drift compensator, $k_p = 300$, $k_i = 37500$, $f_{LPF} = 10$Hz.

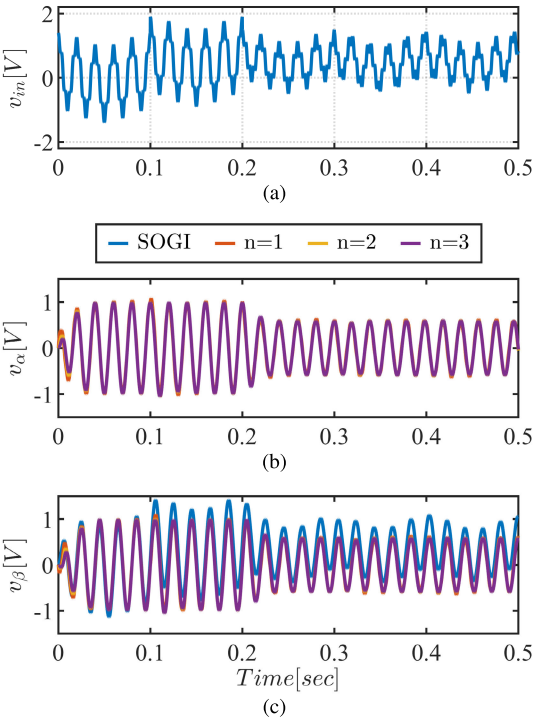

FIGURE 16. (a) Synthesized input voltage, $v_{in} = 1$V, $f_{in} = 50$Hz with 20% of 1/5th and 5th harmonic components, DC offset of 0.5V applied at time = 0.1sec., voltage sag of 40% applied at time = 0.2sec., phase jump of 30 deg. applied at time = 0.3sec., fundamental frequency changes to 52Hz at time = 0.4sec. (b) Direct output of OSGs. (c) Orthogonal output of OSGs.

The input to the 1-D LUT will be the estimated input signal frequency, ω_1. The phase error can be estimated using the transfer function of n^{th}-order BPF OSG in (11). Considering additional phase lead or lag introduced by the phase shifter in (20), δ_{pcn} in (26) is pre-calculated as function of the frequency of the input signal, v_{in}. To avoid increasing the computational burden, 1-dimensional lookup table (1-D LUT) is implemented in FDC as shown in Fig. 14. To reduce the effect of high-frequency noise on the estimated input signal frequency, the integral signal from LF is filtered by a first-order LPF whose cutoff frequency is f_{LPF}.

Figure 15 (a) shows pre-calculated compensation phase as function of input signal frequency for first-, second- and third-order BPF OSGs. Figure 15 (b) shows estimated phase simulation results of the proposed PLL with and without FDC. With FDC, the phase error due to frequency drift is compensated.

$$\delta_{pcn}(\omega_1) = \angle\left(\left(\frac{\frac{\omega_0}{Q_{sn}}(j\omega_1)}{(j\omega_1)^2 + \frac{\omega_0}{Q_{sn}}(j\omega_1) + \omega_0^2}\right)^n\right) + 0.5\left(\angle\left(\frac{\omega_0 - (j\omega_1)}{(j\omega_1) + \omega_0}\right) + \frac{\pi}{2}\right) \quad (26)$$

B. STABILITY ANALYSIS

A linearized model for SOGI-PLL is presented [27]. For a step phase change, the PD output signal can be approximated in Laplace domain as (27) where ϕ_e is the phase error given a sinusoidal input and V_{in} is the input voltage magnitude [11], [27]. The closed-loop transfer function of the PLL in Fig. 14 will be (28). Note that the frequency drift compensator, working as a feedforward, does not affect the stability analysis since it is not part of the closed-loop. The n^{th}-order BPF based model is always stable for any given positive k_p and k_i with all poles being on the left-hand side of the root locus plane.

$$v_{qn}(s) = \frac{V_{in}}{\left(\frac{2Q_{sn}}{\omega_o}s + 1\right)^n}\phi_e(s) \quad (27)$$

$$G_{CL}(s) = \left(\frac{v_{qn}(s)}{\phi_e(s)}\right)\left(\frac{k_p s + k_i}{s^2 + k_p s + k_i}\right) \quad (28)$$

V. SIMULATION AND EXPERIMENTAL RESULTS

In this section, the proposed OSGs, following the design guideline presented in section III., are tested in simulation and experiment. The performance of the proposed OSGs in Fig. 2 (b) is compared with SOGI OSG in Fig. 2 (a). For both simulation and experimental results, Q factor = 2 of OSG order $n = 1$ is selected as the base. For higher order OSGs, scaled Q factor in (22) is used matching -3dB frequency. From (25), the number of oscillations to reach 95% of the steady state is approximately equal to the Q factor. Time

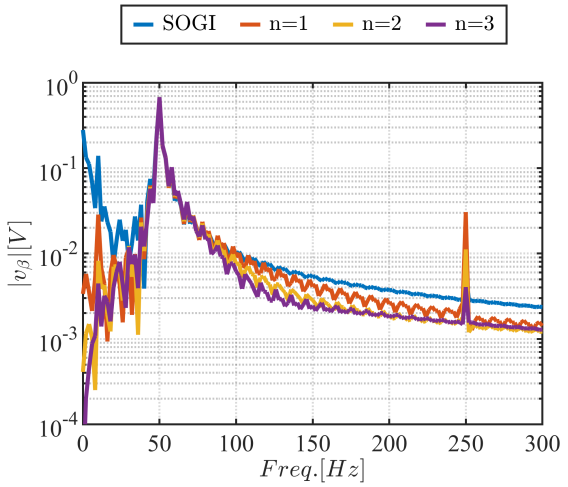

FIGURE 17. Frequency spectrum of the OSG output given v_{in} = 1V, f_{in}=50Hz with 20% of 1/5th and 5th harmonic components, DC offset of 0.5V applied at time = 0.1sec., voltage sag of 40% applied at time = 0.2sec., phase jump of 30deg. applied at time = 0.3sec., fundamental frequency changes to 52Hz at time = 0.4sec.

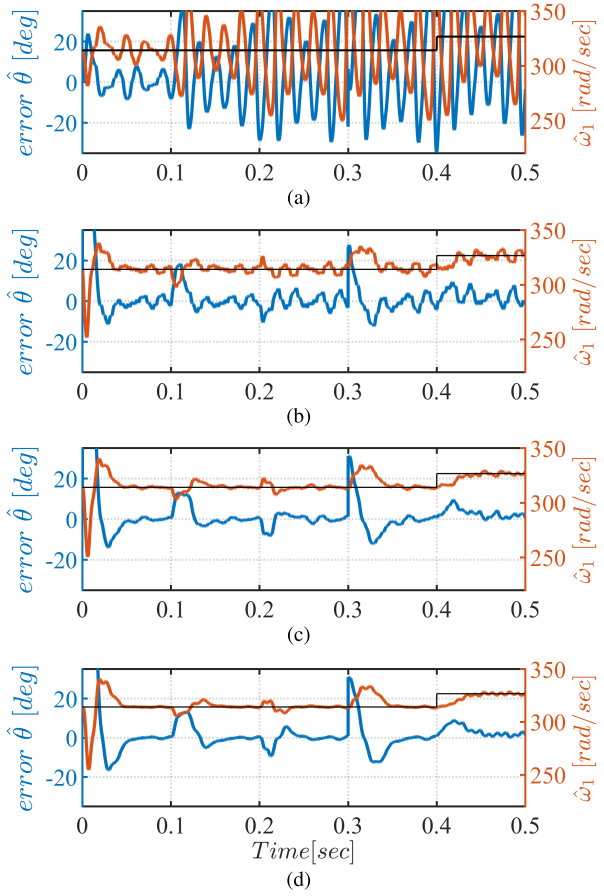

FIGURE 18. PLL estimated phase and frequency simulation results. (a) SOGI-PLL. (b) Proposed OSG-PLL, n = 1. (c) Proposed OSG-PLL, n = 2. (d) Proposed OSG-PLL, n = 3.

required to reach steady-state is 0.05sec given changes in the input using (24) base Q factor of 2.

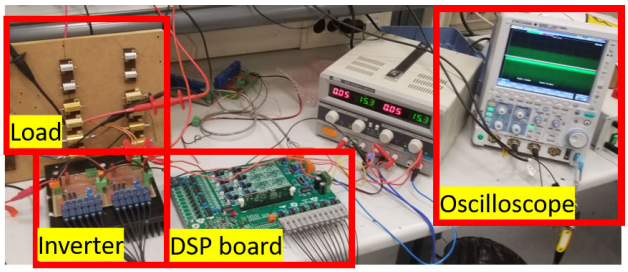

FIGURE 19. Experimental setup.

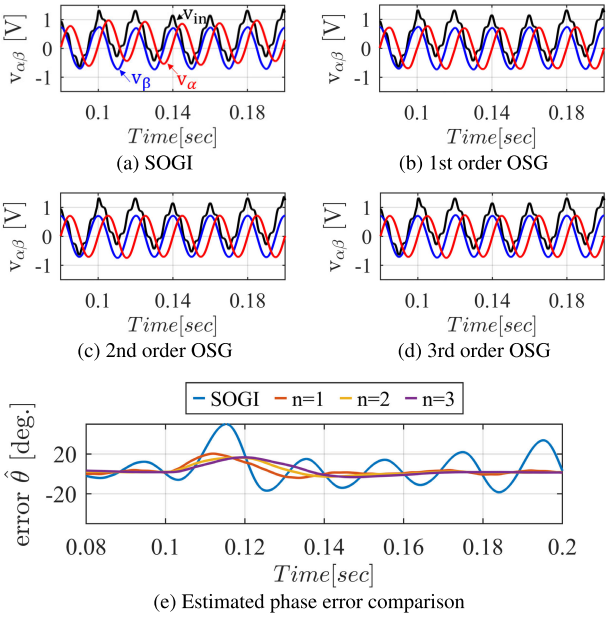

FIGURE 20. Experimental results with DC voltage offset of 0.5V applied at time = 0.1sec., v_{in} synthesized with 1V of 50Hz fundamental frequency with 0.2V of 1/5th and 5th harmonic components, $Q_{(SOGI)} = 2$, $Q_{s1} = 2$, $Q_{s2} = 1.29$, $Q_{s3} = 1.02$, $\omega_0 = 300$rad/sec.

A. SIMULATION RESULTS

Simulation is performed in Simulink environment. The input to OSGs is synthesized as shown in Fig. 16 (a) with the fundamental frequency of 50Hz, including 20% of $1/3^{th}$, $1/5^{th}$ and 5^{th} harmonic components to verify the harmonic filtering capability; $1/3^{th}$ and $1/5^{th}$ harmonic components have been selected to evaluate the low frequency harmonic rejection capability of the proposed OSGs. The DC offset, voltage sag, phase offset, and frequency variation are applied to the input at 0.1sec., 0.2sec., 0.3sec., and 0.4 sec., respectively. The scaled Q_{sn} factors used for the tested OSGs are 2, 2, 1.29, 1.02 for the SOGI, $n = 1$, $n = 2$, $n = 3$ OSGs using (22). The input in Fig. 16 (a) is applied to both SOGI-OSG and proposed OSGs. The resulting direct and orthogonal signals are shown in Figs. 16 (b) and (c). Note that the orthogonal component of SOGI OSG in Fig. 16 (c) result in offset error after DC offset is applied at 0.1sec. The quality of the OSG output is important since they are the input to the PLL for phase and frequency estimation. The frequency spectrum of

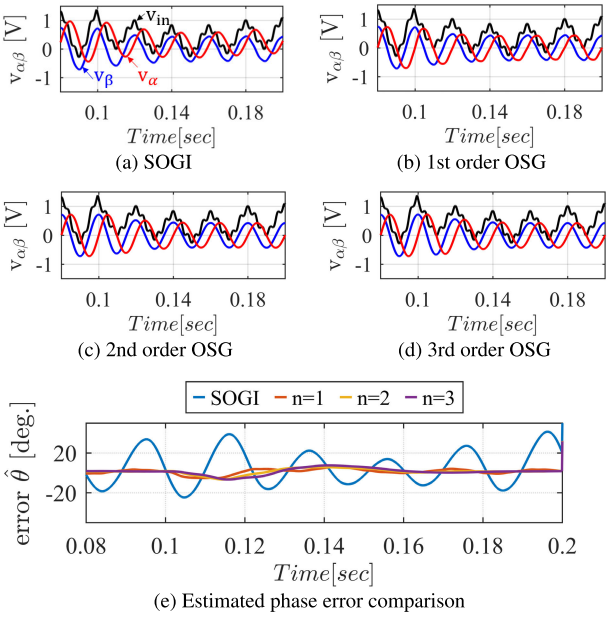

FIGURE 21. Experimental results with 40% voltage sag applied at time = 0.1sec., v_{in} synthesized with 1V of 50Hz fundamental frequency with 0.2V of 1/5th and 5th harmonic components, DC offset of 0.5V, $Q_{(SOGI)} = 2$, $Q_{s1} = 2$, $Q_{s2} = 1.29$, $Q_{s3} = 1.02$.

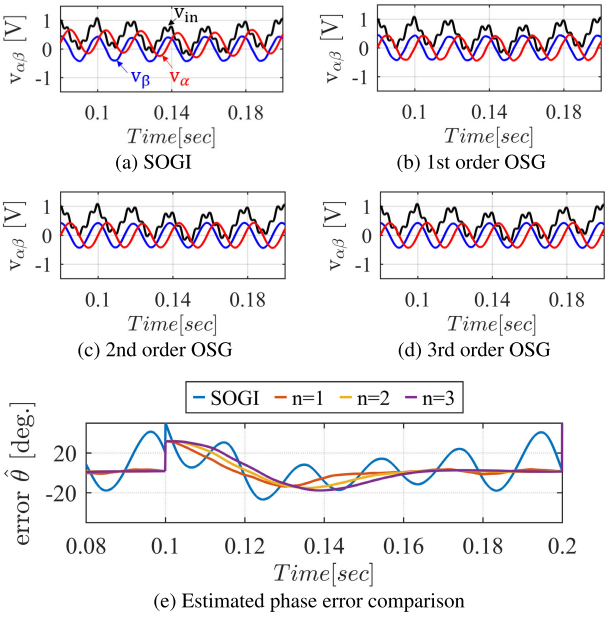

FIGURE 22. Experimental results with 30deg. phase jump applied at time = 0.1sec., v_{in} synthesized with 0.6V of 50Hz fundamental frequency with 0.2V of 1/5th and 5th harmonic components, DC offset of 0.5V, $Q_{(SOGI)} = 2$, $Q_{s1} = 2$, $Q_{s2} = 1.29$, $Q_{s3} = 1.02$.

the orthogonal response from OSGs is shown in Fig. 17, taking the fast Fourier transform (FFT). The interharmonic components, including DC and 5th harmonic component at 250Hz, can be observed from Fig. 17. Enhanced harmonic rejection ability is observed with increasing order of the proposed OSGs.

The estimated phase error and frequency using PLL in Fig. 14 is shown in Fig. 18. The left y-axis represents the estimation error and the right y-axis represents the estimated frequency, ω_1. The input frequency reference is shown in a black-line. It can be observed the enhanced estimation results of phase and frequency with increasing filter order. The error results between PLLs are summarized in Table 2.

B. EXPERIMENTAL RESULTS

This section shows the experimental results of the proposed OSGs and the estimated phase from the PLL. The continuous-domain transfer function is transformed to discrete domain using Tustin method with frequency and pre-warping in (13) and (14). The input voltage is synthesized using Pulse Width Modulation (PWM) programmed in DSP (TMS320F28335) shown in Fig. 19. The measured input voltage is filtered by a low pass filtered with a cutoff frequency of 500Hz. The experimental results with DC offset, voltage sag, phase offset, and frequency offset results are shown in Fig. 20, Fig. 21, Fig. 22, and Fig. 23, respectively. Similar to the simulation results, the OSG performance of higher order BPF can reject harmonic components including DC offset to result in less phase error in transient

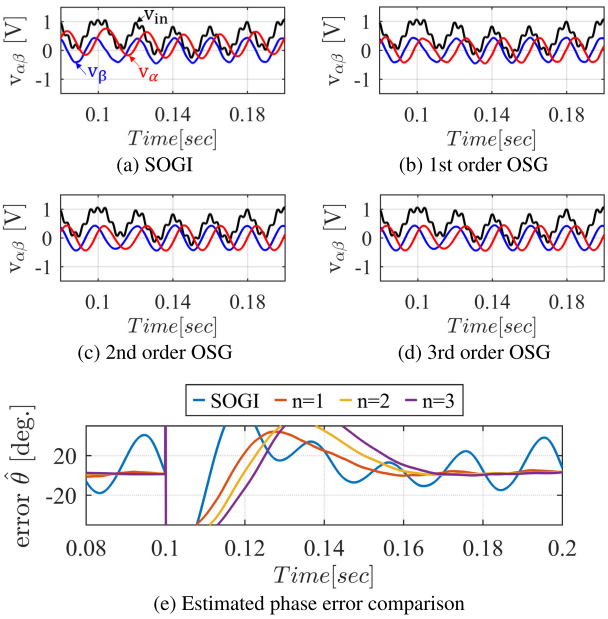

FIGURE 23. Experimental results with frequency drift from 50Hz to 52Hz applied at time = 0.1sec., v_{in} synthesized with 0.6V of 50Hz fundamental frequency with 0.2V of 1/5th and 5th harmonic components, DC offset of 0.5V, $Q_{(SOGI)} = 2$, $Q_{s1} = 2$, $Q_{s2} = 1.29$, $Q_{s3} = 1.02$.

and steady-state. PI gains of PLL are tuned at the nominal frequency of $2\pi 50$[rad/sec] following the procedure in [27].

Summary of the maximum phase error experimental results is shown in TABLE 2. Both the experiment and simulation showed less estimation error with higher order OSGs and comparable settling time.

TABLE 2. Summary of PLL phase error comparison between OSGs in simulation and experimental results.

	PLL OSG	DC Offset		Voltage Sag		Phase Jump		Frequency Variation	
		Transient [deg.]	Steady State [deg.]	Transient [deg.]	Steady State [deg.]	Transient [deg.]	Steady State [deg.]	Transient [deg.]	Steady State [deg.]
Simulation Results	SOGI	36.3	28.84	46.5	30.5	61.5	30.97	60.9	33.8
	n=1	18.3	3.7	10.5	5.8	27.6	5.5	9.4	7.8
	n=2	13.3	0.9	8.2	1.1	31.5	0.4	9.5	2.9
	n=3	13.1	0.6	9.4	0.2	30.9	0.4	9.0	3
Experimental Results	SOGI	50.6	33.2	24.5	17.6	50.5	40.7	86.4	37.6
	n=1	20.37	3.4	5.2	3.3	31.7	3.57	69.3	5.3
	n=2	15.0	1.5	5.6	1.6	31.7	1.9	69.3	2.8
	n=3	14.1	1.4	5.2	1.4	31.7	1.2	69.3	2.3

*All units are in degree.
*Transient error recorded the maximum error at first cycle.
*Steady state error recorded the maximum error at fourth cycle.

VI. CONCLUSION

It has been shown that SOGI-PLL has weakness in the low harmonic rejection capability. To overcome this limitation, this paper presents OSGs with improved harmonic rejection capability based on n^{th}-order BPF and a phase shifter. A scaled Q factor is proposed for the design of higher order OSGs, which simplifies the OSG design process. Frequency- and time-domain analysis are conducted for n^{th}-order BPF OSGs with scaled Q factor. With the scaled Q factor, -3dB frequency and the settling time become compatible for higher order OSGs while enhancing the harmonic rejection capability with -20dB every increasing filter order. The proposed OSGs with scaled Q factor are verified by simulation and experimental results. Higher order OSGs showed higher harmonic rejection capability and comparable settling time with the tradeoff in increasing the computational burden.

REFERENCES

[1] R. M. S. Filho, P. F. Seixas, P. C. Cortizo, L. A. B. Torres, and A. F. Souza, "Comparison of three single-phase PLL algorithms for UPS applications," *IEEE Trans. Ind. Electron.*, vol. 55, no. 8, pp. 2923–2932, Aug. 2008.

[2] J.-W. Choi, Y.-K. Kim, and H.-G. Kim, "Digital PLL control for single-phase photovoltaic system," *IEE Proc. Electr. Power Appl.*, vol. 153, no. 1, pp. 40–46, Jan. 2006.

[3] C. N.-M. Ho, H. S. H. Chung, and K. T. K. Au, "Design and implementation of a fast dynamic control scheme for capacitor-supported dynamic voltage restorers," *IEEE Trans. Power Electron.*, vol. 23, no. 1, pp. 237–251, Jan. 2008.

[4] L. I. Iepure, I. Boldea, and F. Blaabjerg, "Hybrid I-f starting and observer-based sensorless control of single-phase BLDC-PM motor drives," *IEEE Trans. Ind. Electron.*, vol. 59, no. 9, pp. 3436–3444, Sep. 2012.

[5] P. Rodriguez, A. Luna, M. Ciobotaru, R. Teodorescu, and F. Blaabjerg, "Advanced grid synchronization system for power converters under unbalanced and distorted operating conditions," in *Proc. IECON 32nd Annu. Conf. IEEE Ind. Electron.*, Nov. 2006, pp. 5173–5178.

[6] M. McGranaghan, D. Mueller, and M. Samotyj, "Voltage sags in industrial systems," in *Proc. Conf. Record. Ind. Commercial Power Syst. Tech. Conf.*, May 1991, pp. 18–24.

[7] D. Basic, "Input current interharmonics of variable-speed drives due to motor current imbalance," *IEEE Trans. Power Del.*, vol. 25, no. 4, pp. 2797–2806, Oct. 2010.

[8] D. Gallo, R. Langella, A. Testa, and A. Emanuel, "On the effects of voltage subharmonics on power transformers: A preliminary study," in *Proc. 11th Int. Conf. Harmon. Qual. Power*, Sep. 2004, pp. 501–506.

[9] C. Zhang, X. Zhao, X. Wang, X. Chai, Z. Zhang, and X. Guo, "A grid synchronization PLL method based on mixed second- and third-order generalized integrator for DC offset elimination and frequency adaptability," *IEEE J. Emerg. Sel. Topics Power Electron.*, vol. 6, no. 3, pp. 1517–1526, Sep. 2018.

[10] S. Golestan, J. M. Guerrero, and J. C. Vasquez, "Single-phase PLLs: A review of recent advances," *IEEE Trans. Power Electron.*, vol. 32, no. 12, pp. 9013–9030, Dec. 2017.

[11] F. Xiao, L. Dong, L. Li, and X. Liao, "A frequency-fixed SOGI-based PLL for single-phase grid-connected converters," *IEEE Trans. Power Electron.*, vol. 32, no. 3, pp. 1713–1719, Mar. 2017.

[12] M. S. Reza, M. Ciobotaru, and V. G. Agelidis, "Estimation of single-phase grid voltage fundamental parameters using fixed frequency tuned second-order generalized integrator based technique," in *Proc. 4th IEEE Int. Symp. Power Electron. Distrib. Gener. Syst. (PEDG)*, Jul. 2013, pp. 1–8.

[13] M. Ciobotaru, R. Teodorescu, and F. Blaabjerg, "A new single-phase PLL structure based on second order generalized integrator," in *Proc. 37th IEEE Power Electron. Spec. Conf.*, Jun. 2006, pp. 1–6.

[14] P. Rodriguez, R. Teodorescu, I. Candela, A. V. Timbus, M. Liserre, and F. Blaabjerg, "New positive-sequence voltage detector for grid synchronization of power converters under faulty grid conditions," in *Proc. 37th IEEE Power Electron. Spec. Conf.*, Jun. 2006, pp. 1–7.

[15] J. Matas, M. Castilla, J. Miret, L. G. de Vicuna, and R. Guzman, "An adaptive prefiltering method to improve the speed/accuracy tradeoff of voltage sequence detection methods under adverse grid conditions," *IEEE Trans. Ind. Electron.*, vol. 61, no. 5, pp. 2139–2151, May 2014.

[16] Z. Xin, X. Wang, Z. Qin, M. Lu, P. C. Loh, and F. Blaabjerg, "An improved second-order generalized integrator based quadrature signal generator," *IEEE Trans. Power Electron.*, vol. 31, no. 12, pp. 8068–8073, Dec. 2016.

[17] S. Lubura, M. Šoja, S.-A. Lale, and M. Ikic, "Single-phase phase locked loop with DC offset and noise rejection for photovoltaic inverters," *IEE Power Electron.*, vol. 7, no. 9, pp. 2288–2299, 2014.

[18] M. Ciobotaru, R. Teodorescu, and V. G. Agelidis, "Offset rejection for PLL based synchronization in grid-connected converters," in *Proc. 23rd Annu. IEEE Appl. Power Electron. Conf. Expo.*, Feb. 2008, pp. 1611–1617.

[19] M. Karimi-Ghartemani, S. A. Khajehoddin, P. K. Jain, A. Bakhshai, and M. Mojiri, "Addressing DC component in PLL and notch filter algorithms," *IEEE Trans. Power Electron.*, vol. 27, no. 1, pp. 78–86, Jan. 2012.

[20] Y. Han, M. Luo, X. Zhao, J. M. Guerrero, and L. Xu, "Comparative performance evaluation of orthogonal-signal-generators-based single-phase PLL algorithms—A survey," *IEEE Trans. Power Electron.*, vol. 31, no. 5, pp. 3932–3944, May 2016.

[21] S. Prakash, J. K. Singh, R. K. Behera, and A. Mondal, "Comprehensive analysis of SOGI-PLL based algorithms for single-phase system," in *Proc. Nat. Power Electron. Conf. (NPEC)*, Dec. 2019, pp. 1–6.

[22] A. Agarwal and J. Lang, *Foundations of Analog and Digital Electronic Circuits*. Amsterdam, The Netherlands: Elsevier, 2005.

[23] J. W. Nilsson and S. Riedel, *Electric Circuits*. Upper Saddle River, NJ, USA: Prentice-Hall, 2010.

[24] S. Shinnaka, "A robust single-phase PLL system with stable and fast tracking," *IEEE Trans. Ind. Appl.*, vol. 44, no. 2, pp. 624–633, Mar. 2008.

[25] P. Rodríguez, A. Luna, R. S. Muñoz-Aguilar, I. Etxeberria-Otadui, R. Teodorescu, and F. Blaabjerg, "A stationary reference frame grid synchronization system for three-phase grid-connected power converters under adverse grid conditions," *IEEE Trans. Power Electron.*, vol. 27, no. 1, pp. 99–112, Jan. 2012.
[26] H. Zumbahlen, *Linear Circuit Design Handbook*. London, U.K.: Newnes, 2011.
[27] S. Golestan, M. Monfared, F. D. Freijedo, and J. M. Guerrero, "Dynamics assessment of advanced single-phase PLL structures," *IEEE Trans. Ind. Electron.*, vol. 60, no. 6, pp. 2167–2177, Jun. 2013.

YE GU KANG (Member, IEEE) received the B.S. degree in electrical engineering from Penn State University, University Park, PA, USA, in 2011, and the M.S. degree in electrical engineering and the Ph.D. degree in mechanical engineering from the University of Wisconsin–Madison, Madison, WI, USA, in 2013 and 2019, respectively. He is currently an Investigator with the University of Oviedo, Gijon, Spain. His research interest includes design and control of energy conversion devices.

DAVID DIAZ REIGOSA (Member, IEEE) was born in Spain, in 1979. He received the M.E. and Ph.D. degrees in electrical engineering from the University of Oviedo, in 2003 and 2007, respectively. He was a Visiting Scholar with the Wisconsin Electric Machines and Power Electronics Consortium, University of Wisconsin–Madison, Madison, WI, USA, in 2007. He was also a Visiting Professor with the Electrical Machines and Drives Group, The University of Sheffield, U.K., in 2016. He is currently an Associate Professor with the Electrical Engineering Department, University of Oviedo. From 2004 to 2008, he was awarded and fellowship of the Personnel Research Training Program funded by the Regional Ministry of Education and Science of the Principality of Asturias. His research interests include sensorless control of induction motors, permanent magnet synchronous motors, and digital signal processing. He was a recipient of nine IEEE Industry Applications Society Conference and IEEE Energy Conversion Congress and Exposition prize paper awards.